

Efficient Projection onto the $\ell_{\infty,1}$ Mixed-Norm Ball using a Newton Root Search Method

Gustavo Chau¹, Brendt Wohlberg², and Paul Rodriguez¹

¹Electrical Engineering Department, Pontificia Universidad Católica del Perú, Lima, Perú

Email: {gustavo.chau, prodrig}@pucp.edu.pe

²Theoretical Division, Los Alamos National Laboratory, Los Alamos, NM 87545 USA

Email: brendt@lanl.gov

Abstract

Mixed norms that promote structured sparsity have numerous applications in signal processing and machine learning problems. In this work, we present a new algorithm, based on a Newton root search technique, for computing the projection onto the $\ell_{\infty,1}$ ball, which has found application in cognitive neuroscience and classification tasks. Numerical simulations show that our proposed method is between 8 and 10 times faster on average, and up to 20 times faster for very sparse solutions, than the previous state of the art. Tests on real functional magnetic resonance image data show that, for some data distributions, our algorithm can obtain speed improvements by a factor of between 10 and 100, depending on the implementation.

Index Terms

Mixed norms, Structured sparsity, Projection, Regularization, Root-finding

I. INTRODUCTION

Mixed norms are important in modeling group correlations in applications such as genetics [1], electroencephalography [2] and signal processing [3]. In this work, we consider mixed norms with non-overlapping groups applied to matrix-form data $A \in \mathbb{R}^{M \times N}$, where the rows $\mathbf{a}_m \in \mathbb{R}^N$ represent the different groups. Following the notation of [3], we define the $\ell_{p,q}$ -norm of A as

$$\|A\|_{p,q} = \left(\sum_{m=1}^M \|\mathbf{a}_m\|_p^q \right)^{1/q}. \quad (1)$$

We will focus on a special case, the $\ell_{\infty,1}$ -norm:

$$\|A\|_{\infty,1} = \sum_{m=1}^M \|\mathbf{a}_m\|_{\infty}, \quad (2)$$

where $\|\mathbf{u}\|_{\infty} = \max_n \{|u_n|\}$ for $\mathbf{u} \in \mathbb{R}^N$.

The main contribution of this work is a new, computationally efficient algorithm for computing the projection onto the $\ell_{\infty,1}$ -ball:

$$\begin{aligned} \text{proj}_{\|\cdot\|_{\infty,1}}(B, \tau) &:= \arg \min_X \frac{1}{2} \|X - B\|_F^2 \\ \text{s.t. } &\|X\|_{\infty,1} \leq \tau. \end{aligned} \quad (3)$$

This $\ell_{\infty,1}$ constraint problem has been applied to image annotation [4], cognitive neuroscience [5] and least absolute shrinkage and selection operator (LASSO) regression [6]. We propose a novel approach for solving (3) that utilizes a root search based on a Newton method, in which the total number of major iterations for the root search is reduced by applying a simple scheme for choosing a feasible initial solution. This approach provides significantly improved performance compared with our previous approach based on a Steffensen root finding method [7]. The contributions of the present manuscripts can be summarized as:

- (i) We present a new method for solving (3). Instead of a Steffensen root-finding procedure, we formally develop an approximated Newton method for the root search function.
- (ii) We significantly expand the theoretical analysis of the initial point estimation and pruning.
- (iii) We consider additional experiments conducted on real functional magnetic resonance imaging (fMRI) data in order to validate the usefulness of our proposed method.

The manuscripts is organized as follows: Section II summarizes existing approaches for solving (3), Section III presents some mathematical preliminaries needed for our derivations, Section IV describes our proposed method, Sections V and VI present our results on simulated and real data, and in Sections VI-D and VII, we discuss these results and present the conclusions of our work.

II. EXISTING APPROACHES

In this section, we review some previous approaches for solving (3). These methods tend to focus on reinterpreting the problem via some form of quadratic or linear programming (Sections II-A and II-B) or via root-finding (Sections II-D and II-E).

A. Solution via interior point methods

An approach for achieving simultaneous variable selection by considering the problem

$$\begin{aligned} \min_X &\frac{1}{2} \|QX - B\|_F^2 \\ \text{s.t. } &\|X\|_{\infty,1} \leq \tau, \end{aligned} \quad (4)$$

where Q is a fixed matrix and τ is a problem parameter, was proposed in [8]. For the particular case where $Q = I$, this approach consisted of introducing the variables $\rho_m, m \in \{1, \dots, M\}$ and recasting the problem as a convex

quadratic optimization:

$$\begin{aligned}
& \min_{\{\rho_m\}} \frac{1}{2} \sum_{n=1}^N \sum_{m=1}^M (|b_{nm}| - \rho_m)_+^2 \\
& \text{s.t.} \quad \sum_{m=1}^M \rho_m = \tau, \\
& \quad \rho_m \geq 0, \quad m \in \{1, \dots, M\},
\end{aligned} \tag{5}$$

where $(x)_+ = \max(x, 0)$. It was shown that the ρ_l are piecewise linear functions of τ and that they fulfill the Karush-Kuhn-Tucker conditions in each linear section. The algorithm for solving (4) involves starting at 0 and finding the “knots” where the ρ_l change from one linear piece to another, until they encounter a interval containing τ .

B. Solution via linear programming

An equivalent linear program given by:

$$\begin{aligned}
& \text{find} \quad \mu, \theta \\
& \text{s.t.} \quad \sum_n \mu_n = \tau, \\
& \quad \sum_m (A_{nm} - \mu_n)_+ = \theta, \forall n \text{ such that } \mu_n > 0, \\
& \quad \sum_m A_{i,j} \leq \theta, \forall n \text{ such that } \mu_n = 0, \\
& \quad \mu_n \geq 0, \forall n, \\
& \quad \theta \geq 0,
\end{aligned} \tag{6}$$

was derived in [4]. The variables μ_i correspond to the ℓ_∞ -norm values of each row of the optimum solution, and θ is related to a shrinkage parameter associated with the projection onto the ℓ_1 -ball. θ and μ are found via a search procedure over a piece-wise linear function, similar to that of Section II-A.

C. Solution via a dual splitting of the maximum function

The segmentation of an image into K non-overlapping regions can be posed as a spatially regularized version of the K-means problem, i.e. piecewise constant Mumford-Shah problem. Via a lifting-based reformulation [9, Section 2.1], this problem can be expressed as

$$\min_Z \langle Z, W \rangle + \frac{\lambda}{2} \sum_{m=1}^M \text{TV}(\mathbf{z}_m) \quad \text{s.t.} \quad \|Z\|_{\infty,1} \leq K, \tag{7}$$

where $\langle \cdot, \cdot \rangle$ represents the inner product, $\text{TV}(\cdot)$ is any discrete form of Total Variation (TV) [10], λ is the regularization parameter, and Z represents the set of M groups, individually represented by \mathbf{z}_m , each of which as a binary assignment vector, with elements in $\{0, 1\}$ [9, Section 2.1].

In order to avoid a direct solution of the projection onto the $\ell_{\infty,1}$ ball subproblem in (7), [9] made use of the infimal convolution (or epi-sum) representation of the maximum function [11], [9, Eq. (11)], resulting in an splitting approach [9, Eq. (12)] tailored to the particular properties of variable Z . While an adaptation of this method could, in principle, be used to solve (3), such an adaptation is not straightforward, and to the best of our knowledge, has yet to be developed.

D. Projection onto the $\ell_{p,1}$ ball by root search

The general $\ell_{p,1}$ -ball projection problem was solved by means of a root search technique in [6]. This approach relies on the fact that the proximal operator of the $\ell_{p,1}$ norm, defined as

$$\text{prox}_{\|\cdot\|_{p,1}}(B, \lambda) := \arg \min_X \frac{1}{2} \|X - B\|_F^2 + \lambda \|X\|_{p,1}, \quad (8)$$

has a simpler solution than the projection onto the $\ell_{p,1}$ -ball (3), since (8) can be computed by solving independent ℓ_p -norm proximity subproblems [6] of the form

$$\arg \min_{\mathbf{x}_m} \frac{1}{2} \|\mathbf{x}_m - \mathbf{b}_m\|_F^2 + \lambda \|\mathbf{x}_m\|_p. \quad (9)$$

One of the contributions of [6] was to propose a method to take advantage of the separability of (8) in order to solve (3). Let $\mathcal{L}(X, \theta)$ be the Lagrangian of (3), i.e.,

$$\mathcal{L}(X, \theta) = \frac{1}{2} \|X - B\|_F^2 + \theta (\|X\|_{\infty,1} - \tau) \quad (10)$$

and let θ^* be the optimal dual variable. As long as $\tau > 0$, (3) satisfies Slater's conditions for strong duality [12]. Therefore, the primal optimal variable $X^*(\theta^*) = \arg \min_X \mathcal{L}(X, \theta^*)$ can be obtained by computing

$$X^*(\theta^*) = \arg \min_X \frac{1}{2} \|X - B\|_F^2 + \theta^* (\|X\|_{p,1} - \tau). \quad (11)$$

Defining

$$X(\theta) = \text{prox}_{\|\cdot\|_{p,1}}(B, \theta) \quad (12)$$

and scalar function

$$g(\theta) = \|X(\theta)\|_{p,1} - \tau, \quad (13)$$

it can be shown [6, Lemma 2] [13, Lemma 1] that there exist an interval $[0, \theta_{\max}]$ over which $g(\theta)$ is monotonically decreasing and differs in sign at the endpoints. Since θ^* coincides with the unique root of $g(\theta)$, it can be found by using a root finding method.

A root finding method combining bisection, inverse quadratic interpolation, and the secant method was proposed in [6]. This root finding based solution for projections onto the $\ell_{p,1}$ ball was extended to the more general $\ell_{p,q}$ case in a follow-up article [13]. Computational performance comparisons indicated [13, Section 3.1] that this algorithm was both much more accurate and twice as fast as that of [4] for the particular case of projections onto the $\ell_{\infty,1}$ ball.

E. Solution using Steffensen's root-finding method

We have previously presented a technique for solving the $\ell_{1,\infty}$ -constraint problem via a Steffensen root-finding method [7]. Steffensen's method is a quasi-Newton root finding algorithm [14] that is useful when an analytical expression of the derivative is not available. The drawback is that it requires two function evaluations, and is usually more expensive than Newton's method. Given the function $f(x)$, Steffensen's original iterations consist of the update

$$x_{n+1} := x_n + \frac{x_n}{\delta F(x_n, y_n)}, \quad (14)$$

where

$$\delta F(x_n, y_n) = \frac{f(y_n) - f(x_n)}{y_n - x_n} \quad (15)$$

$$y_n = x_n + f(x_n). \quad (16)$$

Steffensen's method tends to exhibit convergence problems if the initial x_0 is too far from the actual root. Therefore, [7] used the modified version proposed in [14]:

$$y_n = x_n + \alpha_n |f(x_n)|.$$

Here α_n is an adaptive parameter that is recommended to take values that satisfy

$$\text{tol}_c \ll \frac{\text{tol}_u}{2|f(x_n)|} < |\alpha_n| < \frac{\text{tol}_u}{|f(x_n)|}, \quad (17)$$

where tol_c is chosen in accordance with the numerical precision used in the implementation, and tol_u is a user-defined parameter.

To the best of our knowledge, the fastest methods for solving the $\ell_{\infty,1}$ -ball projection problem are [4], [6] and [7]. Accordingly, these three algorithms will be used as benchmark for all our comparisons.

III. PRELIMINARIES

A. Notation

We will denote matrices with non-bold upper case font and vectors with bold lower case. Additionally, if $A \in \mathbb{R}^{M \times N}$ is a matrix, we will denote the m^{th} row of A by \mathbf{a}_m , and the i^{th} element of the m^{th} row of A by a_{im} .

B. Projection onto the ℓ_1 -ball

For our proposed solution to (3), we will need to solve the closely related problem of projection onto the ℓ_1 -ball, which is defined as

$$\text{proj}_{\|\cdot\|_1}(\mathbf{u}, \tau) = \arg \min_{\mathbf{x}} \frac{1}{2} \|\mathbf{x} - \mathbf{u}\|_2^2 \quad \text{s.t. } \|\mathbf{x}\|_1 \leq \tau, \quad (18)$$

where $\mathbf{x}, \mathbf{u} \in \mathbb{R}^N$. The solution to this equation is given by [15], [16], [17], [13], [18]

$$\mathbf{x}^* = \begin{cases} \mathbf{u} & \text{if } \|\mathbf{u}\|_1 < \tau \\ \text{shrink}(\mathbf{x}, \lambda(\tau)) & \text{if } \|\mathbf{u}\|_1 \geq \tau, \end{cases} \quad (19)$$

where

$$\text{shrink}(\mathbf{x}, \lambda(\tau)) = \text{sign}(\mathbf{x}) \odot \max(|\mathbf{x}| - \lambda(\tau), 0) , \quad (20)$$

$\lambda(\tau)$ is a shrinkage parameter that depend on τ , and \odot is the element-wise (Hadamard) vector product.

To solve problem (18), we must find λ^* such that $f(\lambda^*) = 0$, where

$$f(\lambda) = \sum_n \max(|u_n| - \lambda, 0) - \tau . \quad (21)$$

Clearly, if $|u_n| > \lambda^*$ then this element contributes to the sum defined in (21); thus, by sorting $|\mathbf{u}|$ in decreasing order, a simple search will lead to the solution: i.e. let $\mathbf{v} = \text{sort}(|\mathbf{u}|)$ and define

$$L = \max \left\{ l \left| l^{-1} \left(\sum_{n=0}^l v_n - \tau \right) < v_l \right. \right\} , \quad (22)$$

then

$$\lambda^* = L^{-1} \left(\sum_{n=0}^L v_n - \tau \right) .$$

This solution was originally described in [19], with several improvements also reported in [20], [21], [15].

The solution of problem (18) can be cast as a root-finding problem, as the function defined in (21) satisfies the Fourier conditions in the interval $[0, u_{\max}]$ and thus has a single root in this interval [16], [22].

The application of the Newton root-finding method [23, Section 11.1]: i.e.

$$\lambda_{k+1} = \lambda_k - \frac{f(\lambda_k)}{f'(\lambda_k)}$$

leads to the so-called Michelot algorithm [24], [25], [16], [22]. More recently, [18], [26], [27] have proposed further improvements to [24].

Since it will be helpful in the derivation of our proposed algorithm (see Section IV), we show how the Michelot algorithm can be derived from a Newton's root-search method applied to (21). This equation can be rewritten as [22, eq. (32)], [26, eq. (7)]:

$$f(\lambda) = \mathbf{z}^T \mathbf{u} - \lambda \mathbf{z}^T \mathbf{z} - \tau , \quad (23)$$

where

$$\mathbf{z} = \text{sign}(\mathbf{u}) \odot I_{|\mathbf{u}| < \lambda} , \quad (24)$$

where $I(\cdot)$ is the indicator function defined for a set A as [28, Chapter 2]:

$$I_A(x) = \begin{cases} 1 & x \in A \\ 0 & x \notin A. \end{cases} \quad (25)$$

Applying the Newton method to (23) by temporarily disregarding the dependence of \mathbf{z} on λ , leads to the Michelot algorithm iterations:

$$\lambda_{k+1} = \lambda_k - \frac{\mathbf{z}_k^T \mathbf{u} - \lambda_k \mathbf{z}_k^T \mathbf{z}_k - \tau}{-\mathbf{z}_k^T \mathbf{z}_k} = \frac{\mathbf{z}_k^T \mathbf{u} - \tau}{\mathbf{z}_k^T \mathbf{z}_k} , \quad (26)$$

where $\mathbf{z}_k^T \mathbf{u}$ is the ℓ_1 norm of the subset of elements of \mathbf{u} for which the corresponding absolute value is greater than λ_k , and $\mathbf{z}_k^T \mathbf{z}_k$ is the number of elements of this subset (equal to the number of non-zero elements in \mathbf{z}_k). Furthermore it can also be shown that

$$0 < \lambda_k \leq \lambda_{k+1} \leq \lambda^* \quad \forall k, \quad (27)$$

where λ^* is the parameter that solves (18). Thus at each iteration we can discard or prune all the elements in \mathbf{u} such that $|u_n| \leq \lambda_k$. Following the guidelines given in [26, Section 3.2.2], a careful implementation of such a pruning strategy can lead to a very efficient computational performance of the Michelot algorithm, as empirically shown in [27, Tables I and II].

C. Dual norm

In this section, we summarize additional theoretical results from [6] that will be useful in the analysis and derivation of the proposed algorithm.

Definition 1: [12] If $\|\cdot\|$ is a norm on \mathbb{R}^m , then the associated dual norm, $\|\cdot\|_*$, is defined as

$$\|\mathbf{z}\|_* \triangleq \sup \{ \mathbf{z}^T \mathbf{x} \mid \|\mathbf{x}\| \leq 1 \} . \quad (28)$$

Lemma 2 (see [6, Lemma 1]): Let $q \geq 1$ and let p^* be its conjugate exponent satisfying $\frac{1}{p} + \frac{1}{p^*} = 1$. Then, the norm $\|\cdot\|_{p^*,\infty}$ is dual to $\|\cdot\|_{p,1}$.

It can be shown via Moreau's decomposition [29], [6] that the dual problem of

$$\text{prox}_{\|\cdot\|_{p^*,\infty}}(B, \lambda) := \arg \min_X \frac{1}{2} \|X - B\|_F^2 + \lambda \cdot \|X\|_{p^*,\infty} , \quad (29)$$

where

$$\|X\|_{p^*,\infty} = \max \{ \|\mathbf{x}_k\|_{p^*} \} ,$$

is the projection onto the $\ell_{p,1}$ ball with radius λ , i.e.,

$$\begin{aligned} \text{proj}_{\|\cdot\|_{p,1}}(B, \lambda) &:= \arg \min_X \frac{1}{2} \|X - B\|_F^2 \\ &\text{s.t. } \|X\|_{p,1} \leq \lambda . \end{aligned} \quad (30)$$

IV. PROPOSED METHOD

A. Leveraging $\text{prox}_{\|\cdot\|_{1,\infty}}(\cdot)$, the dual of $\text{proj}_{\|\cdot\|_{\infty,1}}(\cdot)$

As described in Section II-D, the approach of [6] involved solving (30) via a root finding method applied to (3). Here we consider an alternative reinterpretation that allows us to derive several improvements in the proposed algorithm, as explained in the following section. By the results of Section III-C, the proximal operator of $\ell_{1,\infty}$ is the dual of the projection on the $\ell_{\infty,1}$ ball and vice-versa, then $X^* = \text{proj}_{\|\cdot\|_{\infty,1}}(B, \tau)$, can be written as $X^* = B - A^*$, where

$$\begin{aligned} A^* &= \text{prox}_{\|\cdot\|_{1,\infty}}(B, \tau) \\ &= \arg \min_A \frac{1}{2} \|A - B\|_F^2 + \tau \|A\|_{1,\infty} . \end{aligned} \quad (31)$$

Now, if A^* is known, we can define

$$\gamma^* = \|A^*\|_{1,\infty} = \max_m \{\|\mathbf{a}_m^*\|_1\},$$

and thus, after simple algebraic manipulation, (31) can be written as

$$\arg \min_{\{\mathbf{a}_m\}} \frac{1}{2} \sum_m \|\mathbf{a}_m - \mathbf{b}_m\|_2^2 \quad \text{s.t.} \quad \|\mathbf{a}_m\|_1 \leq \gamma^*, \forall m. \quad (32)$$

Clearly, (32) is separable in \mathbf{a}_m , with the individual problems corresponding to a projection on the ℓ_1 -ball (see Section III-B). Accordingly, if we devise a method for obtaining the optimal γ^* value, then the solution to (31), and therefore to (3), can be easily calculated. The γ^* value can be found by a root finding method, as described in the following section.

B. Search function and solution by Newton's method

As originally proposed in [6], we use $\text{prox}_{\|\cdot\|_{\infty,1}}(\cdot)$ to solve $\text{proj}_{\|\cdot\|_{\infty,1}}(\cdot)$ in (13). Thus, we replace X by $B - A$ in (13) and after simple algebraic manipulations, we obtain

$$f(\gamma) = \sum_{m=1}^M \|\mathbf{b}_m - \mathbf{a}_m(\gamma)\|_{\infty} - \tau, \quad (33)$$

defined for $\gamma \geq 0$. Furthermore, since (33) is equivalent to (13), it also satisfies the Fourier conditions, and thus it has a unique root at γ^* . For a given γ , \mathbf{a}_m is computed using the approach described in (32). As each $\mathbf{a}_m(\gamma)$ corresponds to a projection onto the ℓ_1 -ball, we apply (19) and obtain

$$\mathbf{a}_m(\gamma) = \begin{cases} \mathbf{b}_m & \text{if } \|\mathbf{b}_m\|_1 < \gamma \\ \text{sign}(\mathbf{b}_m) \odot \max(|\mathbf{b}_m| - \lambda_m(\gamma), 0) & \text{if } \|\mathbf{b}_m\|_1 \geq \gamma \end{cases} \quad (34)$$

By substituting (34) into (33), we note that only the terms corresponding to the $\|\mathbf{b}_m\|_1 \geq \tau$ contribute to the sum. Accordingly, at each evaluation of the search function, we can prune the rows of B that do not fulfill this condition, and only perform the projections specified in (34) on the remaining rows. Our numerical experiments show that this pruning strategy can reduce the computational time by half or more. Based on this remark, we can rewrite the search function as:

$$f(\gamma) = \sum_{m \in \mathcal{M}} \|\mathbf{b}_m - \text{sign}(\mathbf{b}_m) \odot \max(|\mathbf{b}_m| - \lambda_m(\gamma), 0)\|_{\infty} - \tau, \quad (35)$$

where \mathcal{M} denotes the set of indexes m where $\|\mathbf{b}_m\|_1 \geq \gamma$. We can reduce this expression further by noting that \mathbf{b}_m can be rewritten in the form $\text{sign}(\mathbf{b}_m) \odot |\mathbf{b}_m|$ and factorizing:

$$f(\gamma) = \sum_{m \in \mathcal{M}} \|\text{sign}(\mathbf{b}_m) \odot (|\mathbf{b}_m| - \max(|\mathbf{b}_m| - \lambda_m(\gamma), 0))\|_{\infty} - \tau \quad (36)$$

$$f(\gamma) = \sum_{m \in \mathcal{M}} \| |\mathbf{b}_m| - \max(|\mathbf{b}_m| - \lambda_m(\gamma), 0) \|_{\infty} - \tau. \quad (37)$$

Now, we turn to the analysis of

$$\beta(\mathbf{b}_m) = ||\mathbf{b}_m| - \max(|\mathbf{b}_m| - \lambda_m(\gamma), 0)||_\infty. \quad (38)$$

We will denote by b_{im} the i^{th} component of the vector \mathbf{b}_m . As all the components of this vector are positive, we can write

$$\beta(\mathbf{b}_m) = \max_i (|b_{im}| - \max(|b_{im}| - \lambda_m(\gamma), 0)). \quad (39)$$

For each component, we have:

$$|b_{im}| - \max(|b_{im}| - \lambda_m(\gamma), 0) = \begin{cases} \lambda_m(\gamma) & \text{if } |b_{im}| > \lambda_m(\gamma) \\ |b_{im}| & \text{if } |b_{im}| \leq \lambda_m(\gamma) \end{cases}. \quad (40)$$

Now, we assert that there exists at least one element b_{jm} such that $|b_{jm}| > \lambda_m(\gamma)$. To prove this, suppose that $|b_{im}| \leq \lambda_m(\gamma)$ for all i . Substituting this assumption into (19), we would have that \mathbf{a}_m^* is zero. As we are only considering terms corresponding to $\|\mathbf{b}_m\|_1 \geq \gamma$ we arrive to a contradiction.

Then, as there exist b_{jm} such that $|b_{jm}| > \lambda_m(\gamma)$

$$|b_{jm}| - \max(|b_{jm}| - \lambda_m(\gamma), 0) = \lambda_m(\gamma).$$

All other elements are in turn less or equal to $\lambda_m(\gamma)$. From this, we conclude that $\beta(\mathbf{b}_m) = \lambda_m(\gamma)$. Thus, we rewrite (37) as

$$f(\gamma) = \sum_{m \in \mathcal{M}} \lambda_m(\gamma) - \tau. \quad (41)$$

As outlined in equation (26) (note that here the sub-indexes have a different interpretation), $\lambda_m(\gamma)$ can be expressed as

$$\lambda_m(\gamma) = \frac{z_k^T \mathbf{b}_m - \gamma}{z_k^T z_k}, \quad (42)$$

where

$$z_m = \text{sign}(\mathbf{b}_m) \odot I_{|\mathbf{b}_m| < \lambda_m(\gamma)},$$

so that (41) becomes

$$f(\gamma) = \sum_{m \in \mathcal{M}} \frac{z_m^T \mathbf{b}_m - \lambda}{z_m^T z_m} - \tau. \quad (43)$$

Both z_m and \mathcal{M} depend on γ , however, similar to the derivation for the Michelot algorithm for ℓ_1 -ball projection [30] presented in Section III-B, we temporarily disregard these dependencies and approximate the derivative of f as

$$\frac{\partial f(\gamma)}{\partial \gamma} \approx - \sum_{m \in \mathcal{M}} \frac{1}{z_m^T z_m}. \quad (44)$$

Thus, the updates of the root-finding procedure can be performed in a Newton-like fashion by setting:

$$\gamma_{n+1} := \gamma_n + \frac{f(\gamma)}{\sum_{m \in \mathcal{M}} \frac{1}{z_m^T z_m}}. \quad (45)$$

Our numerical experiments suggest that, if we update z_k at each iteration, this approximation is good enough for use in a Newton root search method. Similarly to the re-derivation of the Michelot algorithm presented in [30], our method can be understood as a quasi-Newton method in the broad-sense of the term. However, we note that it cannot be readily derived from the application of classical quasi-Newton schemes for root-finding, such as Broyden's or Brent's method [31].

C. Initial Point

From here on, we suppose that

$$\|B\|_{\infty,1} = \sum_{m=1}^M \|\mathbf{b}_m\|_{\infty} > \tau. \quad (46)$$

If $\|B\|_{\infty,1} \leq \tau$ in (3) then the optimal solution is trivial, $X^* = B$. We try to find a point γ_0 such that $f(\gamma_0) > 0$ in (33). Then, as $f(\cdot)$ satisfies the Fourier conditions and is therefore non-increasing in the $[0, \gamma^*]$ interval, we can conclude that $0 \leq \gamma_0 \leq \gamma^*$.

We start by assuming that the ℓ_1 -norm of the j^{th} row of the solution \mathbf{A}^* coincides with $\|\mathbf{A}^*\|_{1,\infty}$, i.e., $\max_m \{\|\mathbf{a}_m\|_1\} = \|\mathbf{a}_j\|_1$. Then, via (31), we can find \mathbf{a}_j as:

$$\mathbf{a}_j = \arg \min_{\mathbf{a}} \frac{1}{2} \|\mathbf{a} - \mathbf{b}_j\|_2^2 + \tau \|\mathbf{a}\|_1 = \text{shrink}(\mathbf{b}_j, \tau). \quad (47)$$

We define $\gamma_0 = \|\text{shrink}(\mathbf{b}_j, \tau)\|_1$ and proceed to show that $f(\gamma_0) > 0$. Separating the sum and using the definition of the shrinkage operator in (33), we can write:

$$f(\gamma_0) = \sum_{m=1}^M \|\mathbf{b}_m - \mathbf{a}_m(\gamma)\|_{\infty} - \tau \quad (48)$$

$$\begin{aligned} f(\gamma_0) = & \|b_j - \text{sign}(b_j) \odot (|b_j| - \max(|b_j| - \tau, 0))\|_{\infty} \\ & + \sum_{m \neq j} \|\mathbf{b}_m - \text{proj}_{\|\cdot\|_1}(\mathbf{b}_m, \gamma_0)\|_{\infty} - \tau. \end{aligned} \quad (49)$$

We can reduce this expression further by noting that b_j can be rewritten in the form $\text{sign}(b_k) \odot |b_k|$ and factorize:

$$f(\gamma_0) = \tau_j(\mathbf{b}_j) + \sum_{m \neq j} \|\mathbf{b}_m - \text{proj}_{\|\cdot\|_1}(\mathbf{b}_m, \gamma_0)\|_{\infty} - \tau, \quad (50)$$

where

$$\tau_j(\mathbf{b}_j) = \| |\mathbf{b}_j| - \max(|\mathbf{b}_j| - \tau, 0) \|_{\infty}. \quad (51)$$

We now turn to the analysis of $\tau_j(\mathbf{b}_j)$. As all the components involved in $\tau_j(\mathbf{b}_j)$ are positive, we can write the norm as the maximum of all the components of the vector. For each component, we have:

$$|b_j^{(i)}| - \max(|b_j^{(i)}| - \tau, 0) = \begin{cases} \tau & \text{if } |b_{ij}| > \tau \\ |b_{ij}| & \text{if } |b_{ij}| \leq \tau. \end{cases} \quad (52)$$

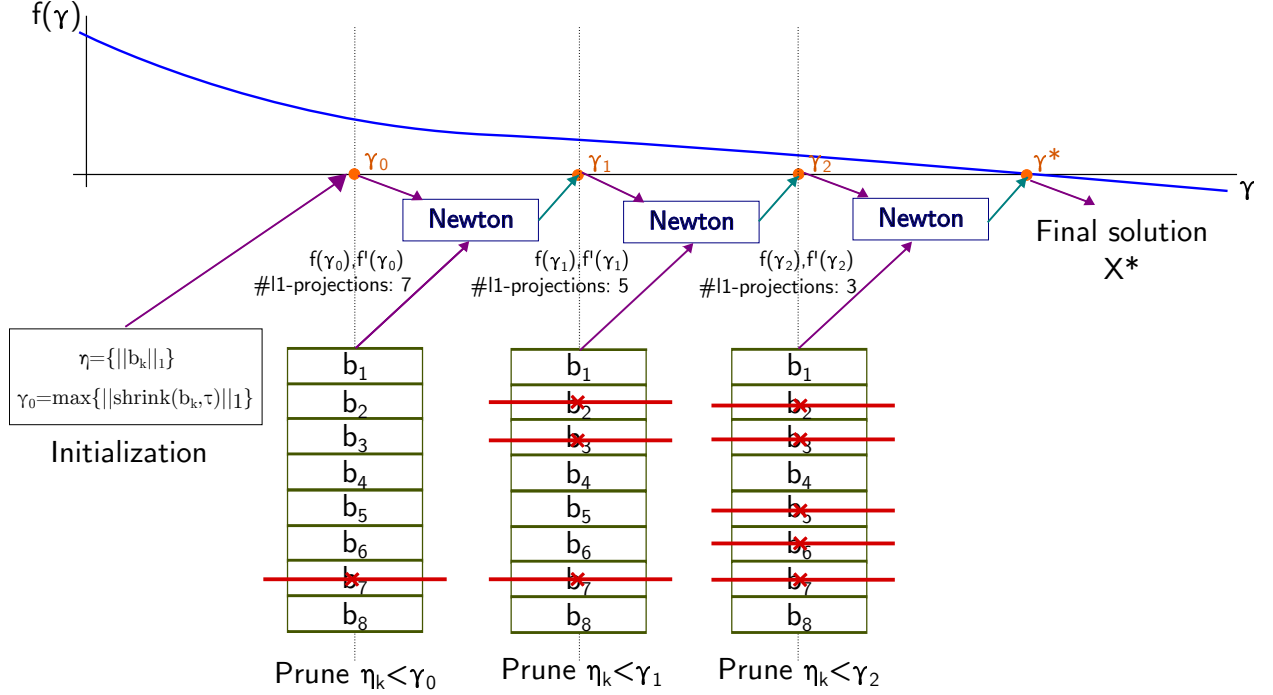


Fig. 1: Diagram illustrating the proposed method for an specific example. The initialization block provides the initial point γ_0 for the root search procedure (see VI-A). At each iteration of γ_n the matrix rows are pruned based on their ℓ_1 -norm as shown in the bottom part of the graphic. The updates of γ_n are done via Newton's method and they converge to the root of the function as shown in the upper part of the graphic (see IV-B)

If we assume that $\|b_j\|_\infty > \tau$, as this is a simple algorithmic check included in our method (See Section IV-D), then at least one of the components of b_j must fulfill the first condition in (52). For at least this component, we have

$$|b_{ij}| - \max(|b_{ij}| - \tau, 0) = \tau, \quad (53)$$

and all the other components are less than or equal to τ . Accordingly,

$$\| |b_j| - \max(|b_j| - \tau, 0) \|_\infty = \tau.$$

Replacing this in (50), we obtain

$$f(\gamma_0) = \sum_{m \neq j} \|b_m - \text{proj}_{\|\cdot\|_1}(b_m, \gamma_0)\|_\infty > 0. \quad (54)$$

Thus, $f(\gamma_0) > 0$ and, instead of starting the root search from 0, we can start from γ_0 , which is a better initial guess of γ^* . *A priori*, we do not know which j is closer to the real maximum. In order to obtain the initial point γ_0 , we solve (47) for every row and then take among these solutions the one with the maximum ℓ_1 -norm.

D. Proposed method

The full proposed method is presented in Algorithm 1 and depicted for an specific example in Figure 1. In line 2, B is checked to see if it is already in the $\ell_{\infty,1}$ -ball. Lines 5 and 6 compute the initial guess of the solution as

outlined in Section IV-C and the initialization Block of Figure 1. Note that if $\|B\|_{\infty,\infty} = \max_{i,j} b_{i,j} < \tau$, lines 5 and 6 do not need to be evaluated and γ is assigned an initial value of 0. Likewise, the shrinkage operation is performed solely for the rows whose ℓ_∞ -norm is greater than τ .

Line 11 corresponds to the pruning step described in Section IV-B, where all rows of B with ℓ_1 norm less than the current γ are discarded. This is also illustrated in the bottom part of the graphic, where the ℓ_1 -projections are not performed on the discarded rows. Lines 12 and 16 perform the approximation of the derivative and the Newton updates (see Section IV-B, Blue Newton blocks in the Figure 1). Line 18 obtains the final \mathbf{A}^* with the last updated γ value and Line 19 returns $B - \mathbf{A}^*$ due to Moreau's decomposition (see Section IV-A).

Algorithm 1: Proposed method via root-finding

```

1
1: if  $\|B\|_{\infty,1} \leq \tau$  then
2:   return  $B$ 
3: end if
4: if  $\|B\|_{\infty,\infty} > \tau$  then
5:   Compute  $\alpha_k = \|\text{shrink}(b_k, \tau)\|_1$  for each row of  $B$ .
6:   Define  $\gamma = \max_k(\alpha_k)$ 
7: else
8:    $\gamma = 0$ .
9: end if
10: for  $k = 1 : \text{maxIter}$  do
11:   Prune the rows of  $B$  that have  $\ell_1$ -norm less than  $\gamma$ 
12:   Obtain  $f(\gamma)$  as defined in (33) and  $\frac{\partial f(\gamma)}{\partial \gamma}$  as defined in (44).
13:   if  $|f(\gamma)| < \text{tolerance}$  then
14:     break
15:   end if
16:   Update  $\gamma$  using Newton method.
17: end for
18: Solve for  $A$  in (32) with the obtained  $\gamma$ .
19: Return  $B - A$ 

```

V. MULTI-TASK LASSO

The Multi-task LASSO (MTL) problem will be used for testing our method on an application involving real data. Let $\text{vec}(\cdot)$ and $\text{vec}^{-1}(\cdot)$ be the vectorization operator and its inverse. Given K tasks, each of length N ordered in

Algorithm 2: Projected gradient descent

```

1  Input: matrix  $B$ , projectionOperator, maxIter, tolerance,  $\alpha$ ,  $W_0$ 
2  Initialization:  $W := W_0$ 
   1: for  $k = 1 : \text{maxIter}$  do
   2:   Compute  $A$  with columns  $A^{(i)} := W_{(k-1)}^{(i)} - \alpha X^T (X W_{(k-1)}^{(i)} - Y^{(i)})$ 
   3:    $W_{(k)} = \text{projectionOperator}(A)$ 
   4:   if  $\|W_{(k)} - W_{(k-1)}\|_F < \text{tolerance}$  then
   5:     break
   6:   end if
   7: end for

```

a $NK \times 1$ vector \mathbf{b} , and a coefficient matrix $W \in \mathbb{R}^{N \times M}$ we want to find the matrix $X \in \mathbb{R}^{M \times K}$ of features that solves

$$\begin{aligned} & \arg \min_X \frac{1}{2} \|\mathbf{b} - P\text{vec}(X)\|_2^2 \\ & \text{subject to } \|X\|_{1,\infty} \leq \tau, \end{aligned} \quad (55)$$

where $P = I_N \otimes W$. The solution of this problem will tend to have few non-zero rows, i.e. selected features. It can be solved by means of projected gradient descent (PGD) [32, Chapter 3], which is shown in Algorithm 2. The method consists of alternating unconstrained gradient descent steps and projections into the $\|X\|_{1,\infty} \leq \tau$ ball. (55) is a convex problem and thus it can be solved using other, more general, optimization methods such as interior point methods [12] or methods based on the augmented Lagrangian function [33].

In this case, projection operator will be a routine that solves (3) by means of our proposed method or via one of the methods in the literature.

VI. RESULTS

All tests presented below were computed using single-threaded Matlab or C-Mex code running on an Intel i7-4770K CPU (8 cores, 2.00 GHz, 32GB RAM). In our simulations with synthetic data (Sections VI-A and VI-B), matrix B was generated using a uniform distribution $[-0.5, 0.5]$, and τ , the constraint used in (2), was taken such that $\tau = \alpha \|B\|_{\infty,1}$, where α is a small constant. Specific sizes of B and values of α are mentioned below. Our Matlab and C code [34] can be used to reproduce our experimental results.

A. Impact of initial point

In order to study the impact of the initial point γ_0 on the performance of the algorithm, we constructed 100 different realizations of a 2000×100 B matrix, considering¹ $\alpha \in [10^{-4}, 10^{-3}]$. For each value of τ , the values

¹These sizes and sparsity values are typical for known applications of (2) [4], [5], [6]. Results for larger values of α can be obtained with our source code [34].

TABLE I: Computational results comparing the effect of the initial point γ_0 . The percent change from the zero-start case is shown in parenthesis for the γ_0 case. *Num. Iter.* represents the average number of iterations across 100 realizations. See Section VI-A.

$\alpha \times 10^{-3}$ / sparsity(%)	Starting at zero		Starting at γ_0	
	num iter	time(s)	num iter	time(s)
0.1 / 1.02	12.6	0.5	9.4 (-25.0%)	0.18 (-65.0%)
0.2 / 1.92	12.2	0.5	9.7 (-19.9%)	0.24 (-52.4%)
0.3 / 2.68	11.9	0.5	10.0 (-16.7%)	0.28 (-44.5%)
0.4 / 3.40	11.7	0.5	10.2 (-12.8%)	0.34 (-32.2%)
0.5 / 4.17	11.5	0.5	11.3 (-2.0%)	0.48 (-5.0%)
0.6 / 4.94	11.3	0.5	11.3 (0.0%)	0.52 (0.3%)
0.7 / 5.53	11.1	0.5	11.1 (0.0%)	0.52 (0.7%)
0.8 / 6.28	11.1	0.5	11.1 (0.0%)	0.52 (0.7%)
0.9 / 6.89	11.0	0.5	11.0 (0.0%)	0.52 (0.6%)
1.0 / 7.53	11.0	0.5	11.0 (0.0%)	0.52 (0.6%)

for the initial point γ_0 and the optimal value γ^* were averaged across the 100 realizations. These average values for each τ are shown in Figure 2(a). It is observed that, at low α values, γ_0 is very close to the optimal value, but it goes rapidly to zero as τ increases. On the other hand, Figure 2(b) shows a comparison of the average number of iterations that the proposed method needs for arriving to the optimal value starting from either zero or γ_0 . The average number of iterations (across 100 realizations) and computational time for the different τ values, for the proposed method without pruning, along with the improvements provided by using γ_0 , are listed in Table I.

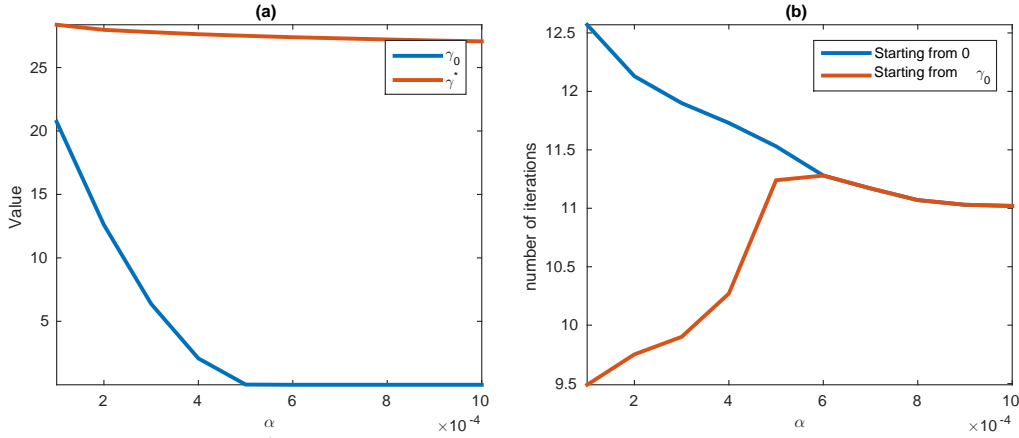


Fig. 2: (a) Value of γ_0 (blue) and γ^* (red) versus α (b) Number of iterations for proposed method to arrive at γ^* starting from 0 (blue) and γ_0 (red) for different α values. See Section VI-A.

B. Simulations

For our first set of experiments, we compared pure matlab implementations of our proposed method (denoted Proposed) against [6], denoted as general root-finding (GRF), and [7], [34], denoted as Steffensen root-finding

TABLE II: Results for simulations with matrices of different size and the three tested methods in pure Matlab code. Error (Err.), number of iterations (N.I.) and running times are shown for each of them. Speedup with respect to GRF is shown for SRF and Proposed. Furthermore, we point out that the error of SRF and Proposed is three to five orders of magnitude lower than that of GRF.

Matrix Size	α / sp	GRF [6]			SRF [7]				Proposed			
		Err.	N.I.	Time(s)	Err.	N.I.	Time(s)	Speedup	Err.	N.I.	Time(s)	Speedup
2 000 x 100	0.0001/ 1.02	3.4e-11	9.6	9.2	2.6e-12	9.4	0.5	17.19	2.0e-16	9.4	0.3	33.54
	0.0005/ 4.13	1.6e-10	13.2	9.5	1.4e-12	11.3	1.7	5.52	7.4e-16	11.3	0.7	13.02
	0.001/ 7.51	5.1e-10	14.5	9.7	1.3e-12	11.0	1.7	5.75	1.5e-15	11.0	0.8	12.38
5 000 x 200	0.0001/ 1.37	1.8e-10	16.9	29.7	1.6e-12	10.6	2.5	11.87	1.0e-15	10.6	1.2	25.82
	0.0005/ 5.59	3.5e-10	17.9	30.9	7.9e-13	12.0	5.1	6.11	2.3e-15	12.0	2.4	12.86
	0.001/ 10.03	7.8e-10	17.9	31.5	6.3e-13	11.1	5.3	5.93	4.6e-15	11.1	2.5	12.64
10 000 x 300	0.0001/ 1.62	5.0e-10	11.4	64.4	9.8e-14	13.0	11.5	5.58	1.9e-15	13.0	5.0	12.86
	0.0005/ 6.6	2.2e-09	14.5	66.4	7.0e-13	12.0	11.5	5.77	9.0e-15	12.0	5.5	12.07
	0.001/ 11.88	3.3e-09	15.7	67.5	2.8e-12	11.4	11.7	5.78	1.9e-12	11.4	5.6	12.02
10 000 x 3 000	0.0001/ 4.24	6.0e-10	20.0	267.5	3.4e-14	13.5	42.6	6.29	4.3e-15	12.99	22.5	11.88
	0.0005/ 16.58	5.7e-10	19.0	264.2	9.0e-14	12.3	41.6	6.35	2.0e-12	11.95	25.0	10.55
	0.001/ 28.51	7.0e-10	18.9	266.3	2.9e-14	12.0	43.9	6.07	5.5e-14	11.01	26.0	10.23
10 000 x 8 000	0.0001/ 6.18	7.0e-09	20.1	594.2	5.6e-14	13.4	94.2	6.31	1.5e-12	13.0	54.8	10.84
	0.0005/ 23.72	2.3e-08	19.2	596.5	1.0e-13	12.4	95.3	6.26	2.4e-12	12.0	61.8	9.66
	0.001/ 39.90	2.4e-08	18.0	584.1	4.0e-14	12.0	98.8	5.91	5.1e-14	11.0	63.1	9.26

TABLE III: Results for simulations with matrices of different size and the three tested methods in C code with mex interface. Error (Err.) and running times are shown for each of them. Speedup with respect to LP is shown for SRF and Proposed. Furthermore, we point out that the error of SRF and Proposed is three to five orders of magnitude lower than that of LP.

Matrix Size	α / sp	LP [4]		SRF [7]			Proposed		
		Err.	Time(s)	Err.	Time(s)	Speedup	Err.	Time(s)	Speedup
2 000 x 100	0.0001/ 1.02	4.2e-10	0.048	2.0e-12	0.007	6.67	1.9e-16	0.005	10.21
	0.0005/ 4.13	4.10e-10	0.046	1.0e-12	0.020	2.30	7.5e-16	0.011	4.17
	0.001/ 7.51	4.1e-10	0.047	1.0e-12	0.022	2.14	1.5e-15	0.012	3.94
5 000 x 200	0.0001/ 1.37	2.6e-08	0.25	1.7e-12	0.055	4.54	6.4e-16	0.033	7.46
	0.0005/ 5.59	2.5e-08	0.25	5.6e-13	0.121	2.04	2.3e-15	0.066	3.75
	0.001/ 10.03	2.5e-08	0.25	6.5e-13	0.123	2.02	4.5e-15	0.067	3.71
10 000 x 300	0.0001/ 1.62	2.3e-07	0.78	8.7e-14	0.352	2.22	1.9e-15	0.19	4.04
	0.0005/ 6.6	2.3e-07	0.78	6.1e-14	0.386	2.02	9.3e-15	0.21	3.73
	0.001/ 11.88	2.3e-07	0.78	3.0e-12	0.393	1.99	1.9e-12	0.21	3.67
10 000 x 3 000	0.0001/ 4.24	2.2e-06	8.95	3.2e-13	4.6356	1.93	4.3e-15	2.51	3.56
	0.0005/ 16.58	2.2e-06	8.95	2.2e-12	5.0528	1.77	2.1e-12	2.72	3.29
	0.001/ 28.51	2.2e-06	8.93	3.9e-13	5.1794	1.72	5.8e-14	2.80	3.19
10 000 x 8 000	0.0001/ 6.18	5.8e-06	25.07	1.7e-12	13.6148	1.84	1.5e-12	7.35	3.41
	0.0005/ 23.72	5.8e-06	25.08	1.9e-12	15.0689	1.66	2.4e-12	8.09	3.10
	0.001/ 39.90	5.8e-06	25.07	3.9e-13	15.5143	1.62	5.3e-14	8.40	2.99

TABLE IV: Mean time in seconds and speedup with respect to GRF for the fMRI experiment (Matlab coded methods).

	GRF [6]	SRF [7]		Proposed	
α / sp	Time(s)	Time(s)	speedup	Time(s)	speedup
0.03/12.5%	1220.7	7.78	156.9	7.75	157.51
0.05/31.4%	1189.3	7.71	154.25	7.66	155.26
0.1/ 58.1%	1109.5	7.89	140.62	7.68	144.47

TABLE V: Mean time in seconds and speedup with respect to LP for the fMRI experiment (C coded methods).

	LP [4]	SRF [7]		Proposed	
α / sp	Time(s)	Time(s)	speedup	Time(s)	speedup
0.03/12.5%	40.3	4.36	9.24	4.36	9.24
0.05/31.4%	39.8	7.86	5.06	7.94	5.01
0.1/ 58.1%	39.9	7.86	5.08	7.92	5.04

(SRF). Unfortunately, we could not find a public implementation of [6], and thus, we coded our own Matlab version using the `fzero` function as root search method as suggested in [6].

For our second set of comparisons, we tested our proposed method implemented in C with a Matlab MEX interface against a similar implementation of SRF [7], [34] and the linear programming (LP) based method described in Section II-B, which was obtained from [35] and also has a MEX interface. None of the C-Mex implementations make use of any type of parallelization (SIMD, CUDA, etc.).

We chose $\text{tol}_c = 10^{-12}$ and $\text{tol}_u = 10^{-8}$ in (17) for the SRF method. The projections onto the ℓ_1 -ball, needed for the evaluation of the search function in [6] and in our algorithm, are implemented using the Michelot algorithm [36]. This algorithm was chosen since it can be implemented efficiently [26, Section 3.2.2],[27, Section 3.1] and, for small size projections, we have empirically observed that it has better computational performance than the alternatives mentioned in Section III-B.

We simulated 100 realizations of five different sizes for the matrix B , namely¹ 2000×100 , 5000×200 , 10000×300 , 10000×3000 and 10000×8000 . For the constraint parameter, we took $\tau = \alpha \|B\|_{\infty,1}$. We considered¹ $\alpha \in \{10^{-4}, 5 \times 10^{-4}, 10^{-3}\}$, to experimentally obtain approximate sparsity percentages (percentage of non-zero rows) of 1, 5 and 10%, respectively.

As discussed in [13], if $\|B\|_{\infty,1} > \tau$ then, at the optimum, the inequality constraint of (3) is active. For all our test, we made sure that $\|B\|_{\infty,1} > \tau$, and thus we measured the error of the solution as $|\|X\|_{\infty,1} - \tau|$. We additionally computed the number of iterations, execution time, and a sparsity value as the percentage of non-zero rows. As all methods arrive to the same value of sparsity, only a single value is shown for each α . The results averaged over the 100 realizations for the different matrix dimensions are shown in Table II and the average speedups are shown in Figure 3.

C. Comparisons on fMRI LASSO application

We tested the computational improvements of our algorithm in the cognitive task described in [37]. The applications consists of predicting the neural functional magnetic resonance image (fMRI) response associated to a

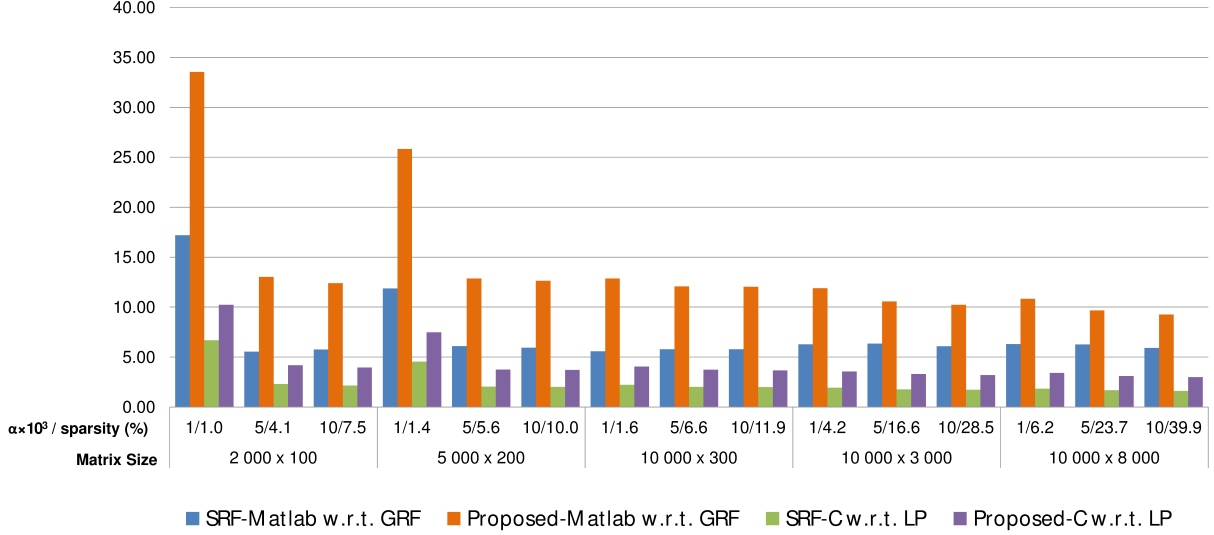


Fig. 3: Bar plot showing the average speedup with respect to GRF for SRF-Matlab (blue), proposed-Matlab (orange), and with respect to LP for SRF-C (green) and Proposed-C (purple) for the different matrix size and α /sparsity values. See also Tables II and III.

particular word based on co-occurrence features of this word with a dictionary of words whose response is already known. In [37], the co-occurrence with a hand-crafted set of 25 verbs was used as features in the prediction problem, whereas [5] showed improvements by using a larger dictionary and MTL to select the best features.

For our tests, we selected the 18 noun words with their corresponding fMRI images and used co-occurrence values of these with a dictionary of 10000 words gathered from Wikipedia and BBC, which was obtained from [38]. These set of 18 words was selected because the other words of the dataset were not present in the corpus used for the co-occurrence matrix calculation.

We subsampled the fMRI images by half resulting in approximate problem dimension of $K = 10000$, $N = 18$ and $M = 10000$. α values of 0.03, 0.05 and 0.1 were considered in order to obtain sparsity values of 12.5%, 31.4% and 58.1%, respectively.

The improvements that can be obtained with the use of mixed norms in MTL has already been demonstrated [5], so we focus only on computational metrics. We compare the time needed to solve (55) by using GRF, SRF and the proposed method as the projection operators in algorithm 2. For PGD, we use the minConf Matlab library [39], [40] which uses an Armijo inexact line search [23] for choosing the step size. We consider a fixed maximum of 40 iterations (due to the long computational times). The results for each case ($\alpha = \{0.03, 0.05, 0.1\}$) are shown in Figure 4 for our proposed method as well as for all other (GRF, SRF and LP) methods; moreover, in Tables IV and V we list the corresponding mean time and speedup for the MATLAB and C coded implementations respectively.

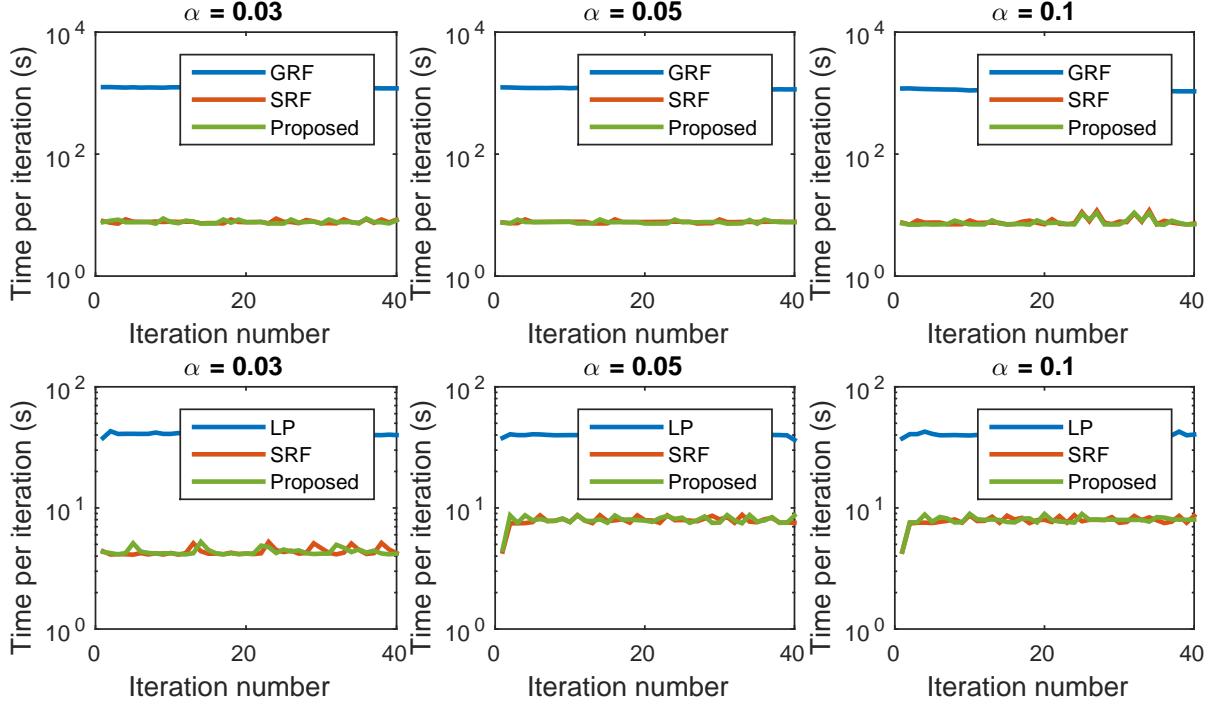


Fig. 4: Time (in seconds) per PGD iteration for each of the methods for solving the $\ell_{\infty,1}$ projection problem associated with the fMRI experiment for Matlab coded methods (Top row) and C coded methods (Bottom row).

D. Discussion

As can be observed from the results of Section VI-A, the initial point γ_0 has impact only at low α (and therefore τ) values. This is easily explainable, as at high τ values the solution of (47) is zero. Accordingly, as suggested in Section IV-D, it is better to first evaluate the conditions on $\max_{n,k} \{b_{n,k}\}$ and $\|\mathbf{b}_i\|_{\infty}$ to avoid unnecessary shrinkage operations, as these comparisons do not incur a great computational cost. When the initial point is different from zero, we see that the number of iterations and the computational time are slightly reduced. For our tests, when γ_0 is not zero, an average reductions of 2.2 iterations (-15%) and of 65% in time are achieved.

As indicated by the results of Section VI-B, the proposed Newton method tends to require fewer iterations than GRF [6], although this is not directly comparable as the stopping criteria of the fzero function used in GRF (only implemented in Matlab) is different from the one we are using in 1 (implemented in Matlab and C-MEX) and because our proposed algorithms are obtaining smaller errors. Additionally, the Newton-based method performs the same number of iterations as the SRF method [7], but the computational time is substantially lower. This is explained by the fact that in the Newton-based method, only one function evaluation is performed compared to the two evaluations performed for the SRF method. Overall, the proposed Newton-based algorithm obtains speedups of 8 or more with respect to GRF (compared to the average of 5 obtained with SRF). Higher speedups are obtained

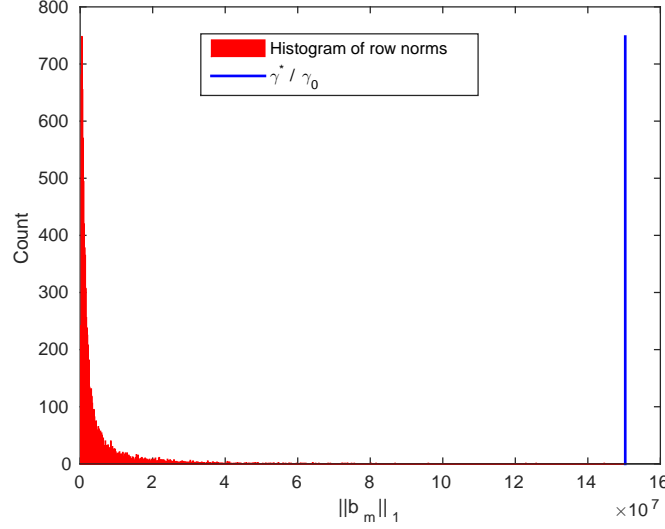


Fig. 5: Distribution of $\|\mathbf{b}_m\|_1$ values (red) and optimal γ value (blue).

at low α (sparser) values, as this is where the initial point guess is more effective [7]. For those cases, the speedup of our proposed method goes up to $14 \sim 25$. Likewise, in the C code comparisons, our proposed method obtained speedups of $3 \sim 10$ with respect to that of LP. The same effect of the initial point guess providing higher speedups at lower α values is also observed.

Regarding the fMRI experiments, we observe that both our previous SRF method and our novel Newton-based methods obtain considerable speedups of $120 \sim 130$. This speedup reduced the total computational time for the whole PGD method from around 10 hours (GRF) to approximately 3 minutes (SRF and Proposed). In the C-code comparisons, we obtained speedups of $5 \sim 9$ with respect to the LP method. The difference in performance with respect to the simulations is explained by the data distribution. As observed in Figure 5, the ℓ_1 -norms of the rows of the data follow a Laplacian-like distribution, while the simulations considered uniformly distributed data. Accordingly, in the fMRI data, the pruning strategy mentioned in Section IV-B is able to greatly reduce the number of rows to be processed. Furthermore, the initial guess γ_0 obtained with the SRF and proposed methods is very close to the optimal γ^* , and so we noticed that only around two root-search iterations were needed for each projection. Although for this particular dataset the proposed method performs comparably to SRF, the simulations showed that for setting where the data is more uniformly distributed the difference in computation can be considerable.

VII. CONCLUSION

We have presented a new algorithm for efficient projection onto the $\ell_{\infty,1}$ -norm ball which exploits the particular structure of this problem to improve over previous methods. The algorithm, based on a Newton root-finding approach, capitalizes on an approximation of the derivative of the search function obtained from Moreau's decomposition and duality theory. Our proposed method obtains speedups of eight or more with respect to previous state-of-the-art methods, while achieving smaller errors in our simulations. When we applied our proposed algorithm to a multi-

task Lasso (MTL) using real fMRI data, we obtained considerable speedups. Furthermore, the MTL test also highlights the impact of two key aspects of our proposed algorithm, namely our initial guess and the pruning steps. When the distribution of the data is favorable, these aspects have a very significant positive impact on the overall computational performance of our proposed algorithm. Implementations of the proposed algorithms in both Matlab and C are provided in [34], and a Python implementation will be included in a future release of the SPORCO library [41]. The data and scripts necessary for reproducing the experiments reported here are also available in [34].

ACKNOWLEDGMENT

This research was supported by the “Programa Nacional de Innovación para la Competitividad y Productividad” (Innóvate Perú) Program, 169-Fondecyt-2015, and by the U.S. Department of Energy through the LANL/LDRD Program.

REFERENCES

- [1] L. Yuan, J. Liu, and J. Ye, “Efficient methods for overlapping group lasso,” in *Advances in Neural Information Processing Systems*, 2011, pp. 352–360.
- [2] A. Gramfort, M. Kowalski, and M. Hämmäläinen, “Mixed-norm estimates for the M/EEG inverse problem using accelerated gradient methods,” *Physics in medicine and biology*, vol. 57, no. 7, p. 1937, 2012.
- [3] M. Kowalski, “Sparse regression using mixed norms,” *Applied and Computational Harmonic Analysis*, vol. 27, no. 3, pp. 303–324, 2009.
- [4] A. Quattoni, X. Carreras, M. Collins, and T. Darrell, “An efficient projection for $\ell_{1,\infty}$ regularization,” in *Proceedings of the 26th Annual International Conference on Machine Learning*. ACM, 2009, pp. 857–864.
- [5] H. Liu, M. Palatucci, and J. Zhang, “Blockwise coordinate descent procedures for the multi-task lasso, with applications to neural semantic basis discovery,” in *Proceedings of the 26th Annual International Conference on Machine Learning*. ACM, 2009, pp. 649–656.
- [6] S. Sra, “Fast projections onto $\ell_{1,q}$ -norm balls for grouped feature selection,” *Machine learning and knowledge discovery in databases*, pp. 305–317, 2011.
- [7] G. Chau, B. Wohlberg, and P. Rodriguez, “Fast projection onto the $\ell_{\infty,1}$ -mixed norm ball using Steffensen root search,” in *International Conference on Acoustics, Speech and Signal Processing (ICASSP)*, 2018, pp. 4694–4698.
- [8] B. A. Turlach, W. N. Venables, and S. J. Wright, “Simultaneous variable selection,” *Technometrics*, vol. 47, no. 3, pp. 349–363, 2005.
- [9] L. Condat, “A convex approach to k-means clustering and image segmentation,” in *EMMCVPR 2017: Energy Minimization Methods in Computer Vision and Pattern Recognition*. Springer International Publishing, 2017, pp. 220–234.
- [10] L. Rudin, S. Osher, and E. Fatemi, “Nonlinear total variation based noise removal algorithms,” *Phys. D*, vol. 60, no. 1-4, pp. 259–268, Nov. 1992.
- [11] H. Bauschke and P. Combettes, *Convex Analysis and Monotone Operator Theory in Hilbert Space*. Springer Berlin, Jan. 2011.
- [12] S. Boyd and L. Vandenberghe, *Convex Optimization*. New York, NY, USA: Cambridge University Press, 2004.
- [13] S. Sra, “Fast projections onto mixed-norm balls with applications,” *Data Mining and Knowledge Discovery*, vol. 25, no. 2, pp. 358–377, Sep. 2012.
- [14] S. Amat, S. Busquier, Á. Magreñán, and L. Orcos, “An overview on Steffensen-type methods,” in *Advances in Iterative Methods for Nonlinear Equations*. Springer, 2016, pp. 5–21.
- [15] J. Duchi, S. Shalev-Shwartz, Y. Singer, and T. Chandra, “Efficient projections onto the ℓ_1 -ball for learning in high dimensions,” in *ICML*, 2008, pp. 272–279.
- [16] J. Liu and J. Ye, “Efficient Euclidean projections in linear time,” in *Proceedings of the International Conference on Machine Learning (ICML)*, 2009, pp. 657–664.
- [17] S. Sra, “Generalized proximity and projection with norms and mixed-norms,” Max Planck Institute for Biological Cybernetics, Tübingen, Germany, Tech. Rep. 192, May 2010.
- [18] L. Condat, “Fast projection onto the simplex and the ℓ_1 ball,” *Mathematical Programming*, vol. 158, no. 1-2, pp. 575–585, 2016.
- [19] M. Held, P. Wolfe, and H. Crowder, “Validation of subgradient optimization,” *Math. Program.*, vol. 6, no. 1, pp. 62–88, 1974.

- [20] E. van den Berg and M. Friedlander, “Probing the Pareto frontier for basis pursuit solutions,” *SIAM Journal on Scientific Computing*, vol. 31, no. 2, pp. 890–912, 2009.
- [21] K. Kiwiel, “Breakpoint searching algorithms for the continuous quadratic knapsack problem,” *Mathematical Programming*, vol. 112, no. 2, pp. 473–491, 2008.
- [22] P. Gong, K. Gai, and C. Zhang, “Efficient Euclidean projections via piecewise root finding and its application in gradient projection,” *Neurocomputing*, vol. 74, no. 17, pp. 2754–2766, 2011.
- [23] J. Nocedal and S. J. Wright, *Numerical Optimization*, 2nd ed. New York, NY, USA: Springer, 2006.
- [24] C. Michelot, “A finite algorithm for finding the projection of a point onto the canonical simplex of \mathbb{R}^n ,” *J. Optim. Theory Appl.*, vol. 50, no. 1, pp. 195–200, 1986.
- [25] K. Kiwiel, “Variable fixing algorithms for the continuous quadratic knapsack problem,” *Journal of Optimization Theory and Applications*, vol. 136, no. 3, pp. 445–458, 2008.
- [26] P. Rodríguez, “An accelerated Newton’s method for projections onto the ℓ_1 -ball,” in *IEEE International Workshop on Machine Learning for Signal Processing (MSLP)*, 2017, pp. 1–6.
- [27] P. Rodriguez, “Accelerated gradient descent method for projections onto the ℓ_1 -ball,” in *IEEE Image, Video, and Multidimensional Signal Processing (IVMSP)*, Jun. 2018, pp. 1–5.
- [28] G. Folland, *Real Analysis: Modern Techniques and Their Applications*, ser. Pure and Applied Mathematics: A Wiley Series of Texts, Monographs and Tracts. Wiley, 2013.
- [29] N. Parikh, S. Boyd *et al.*, “Proximal algorithms,” *Foundations and Trends in Optimization*, vol. 1, no. 3, pp. 127–239, 2014.
- [30] R. Cominetti, W. F. Mascarenhas, and P. J. Silva, “A Newton’s method for the continuous quadratic knapsack problem,” *Mathematical Programming Computation*, vol. 6, no. 2, pp. 151–169, 2014.
- [31] S. C. Chapra and R. Canale, *Numerical Methods for Engineers*, 5th ed. New York, NY, USA: McGraw-Hill, Inc., 2006.
- [32] D. Bertsekas, *Nonlinear Programming*. Athena Scientific, 1999.
- [33] Y. Xu, “First-order methods for constrained convex programming based on linearized augmented lagrangian function,” *arXiv preprint arXiv:1711.08020*, 2017.
- [34] G. Chau and P. Rodriguez, “Matlab codes for projection onto the $\ell_{1,\infty}$ -mixed norm ball,” <https://goo.gl/TngGrc>.
- [35] Ariadna Quattoni, “L1Inf projection Matlab code,” <http://www.lsi.upc.edu/~aquattoni/CodeToShare/L1InfProjection.tar.gz>.
- [36] C. Michelot, “A finite algorithm for finding the projection of a point onto the canonical simplex of \mathbb{R}^n ,” *Journal of Optimization Theory and Applications*, vol. 50, no. 1, pp. 195–200, 1986.
- [37] T. M. Mitchell, S. V. Shinkareva, A. Carlson, K.-M. Chang, V. L. Malave, R. A. Mason, and M. A. Just, “Predicting human brain activity associated with the meanings of nouns,” *science*, vol. 320, no. 5880, pp. 1191–1195, 2008.
- [38] Dissect Toolkit, clic.cimec.unitn.it/composes/toolkit/.
- [39] M. Schmidt, E. Berg, M. Friedlander, and K. Murphy, “Optimizing costly functions with simple constraints: A limited-memory projected quasi-newton algorithm,” in *Artificial Intelligence and Statistics*, 2009, pp. 456–463.
- [40] M. Schmidt, “minconf: projection methods for optimization with simple constraints in Matlab,” <https://goo.gl/NmFePs>.
- [41] B. Wohlberg, “SParse Optimization Research COde (SPORCO),” Software library available from <http://purl.org/brendt/software/sporco>, 2016.